Interactions of WASp, myosin-I, and verprolin with Arp2/3 complex during actin patch assembly in fission yeast

Vladimir Sirotkin,[1] Christopher C. Beltzner,[1] Jean-Baptiste Marchand,[4] and Thomas D. Pollard[1,2,3]

Departments of [1]Molecular Cellular and Developmental Biology, [2]Molecular Biophysics and Biochemistry, and [3]Cell Biology, Yale University, New Haven, CT 06520
[4]Avidis, Biopole Clermont-Limagne, 63360 Saint Beauzire, France

Yeast actin patches are dynamic structures that form at the sites of cell growth and are thought to play a role in endocytosis. We used biochemical analysis and live cell imaging to investigate actin patch assembly in fission yeast *Schizosaccharomyces pombe*. Patch assembly proceeds via two parallel pathways: one dependent on WASp Wsp1p and verprolin Vrp1p converges with another dependent on class 1 myosin Myo1p to activate the actin-related protein 2/3 (Arp2/3) complex. Wsp1p activates Arp2/3 complex via a conventional mechanism, resulting in branched filaments. Myo1p is a weaker Arp2/3 complex activator that makes unstable branches and is enhanced by verprolin. During patch assembly in vivo, Wsp1p and Vrp1p arrive first independent of Myo1p. Arp2/3 complex associates with nascent activator patches over 6–9 s while remaining stationary. After reaching a maximum concentration, Arp2/3 complex patches move centripetally as activator proteins dissociate. Genetic dependencies of patch formation suggest that patch formation involves cross talk between Myo1p and Wsp1p/Vrp1p pathways.

Introduction

During interphase, yeast cells contain two cytoskeleton structures composed of actin filaments, cables that depend on formins and actin patches that depend on the actin-related protein 2/3 (Arp2/3) complex for their formation (Chang and Peter, 2002; Weaver et al., 2003). Actin patches are highly dynamic, mobile structures (Doyle and Botstein, 1996; Waddle et al., 1996; Pelham and Chang, 2001; Smith et al., 2001) that form at the sites of active cell growth and may play a role in endocytosis (Mulholland et al., 1994). Budding yeast form patches at sites of endocytosis where actin assembly may either assist in severing the endocytic membrane or propel the vesicle toward cell interior (Munn, 2001; Engqvist-Goldstein and Drubin, 2003; Kaksonen et al., 2003; Huckaba et al., 2004; Jonsdottir and Li, 2004; Merrifield, 2004). Actin assembly is proposed to play similar roles in endocytosis in cultured vertebrate cells and *Xenopus* eggs (Merrifield et al., 2002; Sokac et al., 2003).

Yeast actin patches share many components involved in extension of the leading edge in motile cells (Pollard et al., 2000; Higgs and Pollard, 2001). Initiation of patch assembly in budding yeast involves coordinated activity of class 1 myosins Myo3p and Myo5p (Goodson et al., 1996; Anderson et al., 1998) and Wiskott-Aldrich Syndrome protein (WASp) family Las17p/Bee1p (Li, 1997). Both Las17p/Bee1p and myosins Myo3p/Myo5p have COOH-terminal domains with a tryptophan and a cluster of acidic residues that bind Arp2/3 complex (Higgs and Pollard, 2001; Weaver et al., 2003). Las17p/Bee1p and myosins Myo3p/Myo5p are genetically and functionally redundant because a single acidic domain either on a myosin-I or Las17p/Bee1p suffices to induce actin patch assembly (Evangelista et al., 2000; Lechler et al., 2000). Actin patch assembly in budding yeast also involves a proline-rich protein, verprolin Vrp1p (Donnelly et al., 1993; Munn et al., 1995; Vaduva et al., 1997), which interacts with both Las17p/Bee1p and Myo3p/Myo5p (Anderson et al., 1998; Naqvi et al., 1998; Evangelista et al., 2000). Vrp1p exists in complex with Las17p (Lechler et al., 2001), and Vrp1p binding to type I myosins is needed to induce actin assembly in cell extracts (Geli et al., 2000). Class I myosins can also bind Las17p/Bee1p directly (Evangelista et al., 2000; Lechler et al., 2000). Interactions among activators may potentially lead to the formation of a large protein complex (Evangelista et al., 2000; Lechler et al., 2000, 2001) and coordinate the recruitment and activation of the Arp2/3 complex.

Correspondence to Thomas D. Pollard: thomas.pollard@yale.edu

Abbreviations used in this paper: Arp2/3, actin-related protein 2/3; CA, central-acidic; mGFP, monomeric GFP; N-WASP, neuronal WASp; SH3, Src homology 3; TH, tail homology; WASp, Wiskott-Aldrich Syndrome protein; WH2, WASp homology 2.

The online version of this article includes supplemental material.

The Journal of Cell Biology, Vol. 170, No. 4, August 15, 2005 637–648
http://www.jcb.org/cgi/doi/10.1083/jcb.200502053

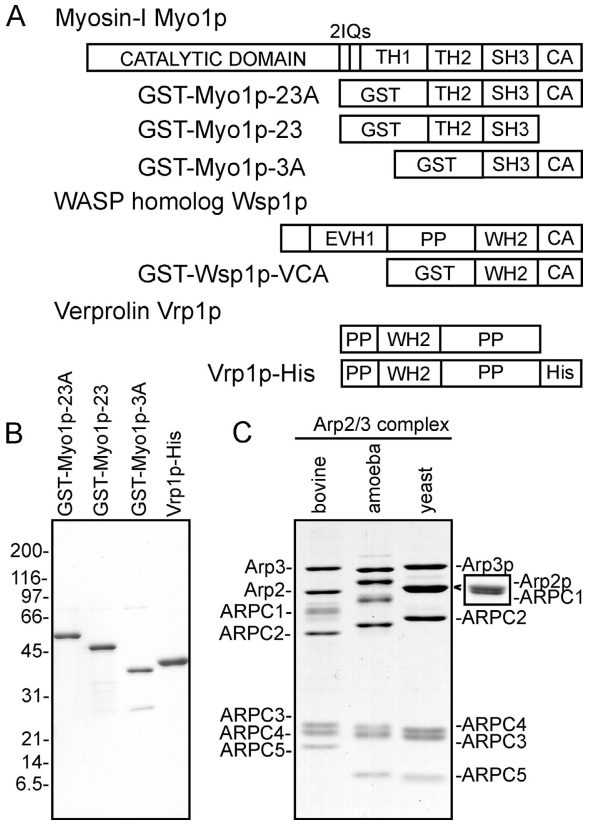

Figure 1. **Proteins used in this study.** (A) A schematic diagram of *S. pombe* Myo1p, Wsp1p, and Vrp1p and their recombinant fusions to GST or a His-tag. (B and C) SDS-PAGE of purified proteins stained with Coomassie blue. (B) Recombinant fusion proteins were purified by affinity and ion exchange chromatography. Molecular weights are indicated on the left. (C) Arp2/3 complex from bovine thymus, *Acanthamoeba*, and fission yeast. An inset shows separation of Arp2p and ARPC1 on a gel loaded with less total protein.

Fission yeast actin patches also depend on myosin-I and WASp (Lee et al., 2000). Like other WASp family members, *Schizosaccharomyces pombe* Wsp1p has a COOH-terminal VCA region with a central-acidic (CA) domain expected to bind Arp2/3 complex and a WASp homology 2 (WH2) domain (V) expected to bind actin monomer (Fig. 1 A), both required to activate Arp2/3 complex in other cells (Higgs and Pollard, 2001). *S. pombe* Myo1p is a long-tailed class 1 myosin with a motor domain, 2 IQ motifs, and a tail that includes a tail homology 1 (TH1) domain expected to bind lipids, a TH2 domain of unknown function, an Src homology 3 (SH3) domain expected to bind proline-rich sequences, and a CA domain (Fig. 1 A). *S. pombe* Vrp1p is a proline-rich protein with an NH_2-terminal WH2 domain. A GST fusion to Myo1p TH2-SH3-CA binds and activates bovine and *Acanthamoeba* Arp2/3 complex (Lee et al., 2000). However, activation is weak, perhaps due to the lack of a WH2 domain to bind an actin monomer.

Fission yeast survive deletion of either the single myosin-I gene *myo1*$^+$ or the single WASp family gene *wsp1*$^+$ with severe cytoskeletal defects, but deletion of both genes is lethal (Lee et al., 2000). Therefore, Myo1p and Wsp1p may have independent but overlapping functions and likely operate in two parallel pathways of actin assembly. Normal patch assembly may rely on coordinated activity of pathways involving Myo1p and Wsp1p, perhaps by direct physical interactions among activators.

Here, we use live cell imaging and genetic analysis in combination with biochemical analysis of purified *S. pombe* Arp2/3 complex, Myo1p tail, Wsp1p VCA, and full-length Vrp1p to study the mechanism of actin patch assembly.

Table I. **Equilibrium dissociation constants (K_d) for interactions among Myo1p tail, Wsp1p VCA, verprolin, Arp2/3 complex, and actin**

Receptor	Ligand	Binding	K_d (μM)
GST-Myo1p-23A	Arp2/3 complex	+	1.2/1.8
GST-Myo1p-3A	Arp2/3 complex	+	2.0/2.1
GST-Myo1p-23	Arp2/3 complex	–	
GST-Wsp1p-VCA	Arp2/3 complex	+	0.05
GST-Myo1p-23A	Verprolin	+	4.6/5.6[a] (3–6 μM)
GST-Myo1p-3A	Verprolin	+	N.D.
GST-Myo1p-23	Verprolin	+	N.D.
Vrp1p-His	G-actin	+	1.0/0.9/0.8

Equilibrium dissociation constants were measured using quantitative pull-down assays. Slashes separate values from independent experiments. N.D., not determined.
[a]Values represent the best fits, the range of values from all fit attempts is in parentheses.

Results

Purification and interactions of Arp2/3 complex, Myo1p, Wsp1p, and Vrp1p

We used affinity and ion exchange chromatography to purify native *S. pombe* Arp2/3 complex and the following recombinant fusion proteins: GST fused to the TH2-SH3-CA, TH2-SH3, and SH3-CA domains of the myosin-I (Myo1p) tail (GST-Myo1p-23A, -23, -3A); GST fused to the VCA region of Wsp1p (GST-Wsp1p-VCA); and full-length verprolin (Vrp1p) with a COOH-terminal His-tag (Fig. 1). *S. pombe* Arp2/3 complex consists of seven subunits (Fig. 1 C) with slightly different electrophoretic mobilities than the subunits in other species. *S. pombe* Arp2p and ARPC1 have similar electrophoretic mobilities. Mass spectrometry identified ARPC3 as the faster migrating subunit in the ~20-kD ARPC3/ARPC4 doublet.

We measured the affinities of these proteins for each other and for actin monomers with quantitative bead pull-down assays (Fig. 2 and Table I). Interaction of the Myo1p tail with Arp2/3 complex depended on the A domain, but not the TH2 domain. Like human GST-WASp-VCA (Hufner et al., 2001), GST-Wsp1p-VCA bound Arp2/3 complex much stronger (K_d ~0.05 μM) than GST-Myo1p-23A (K_d = 1–2 μM). GST-Myo1p-23A bound Vrp1p with a higher affinity (K_d = 3–6 μM) than muscle actin monomers or filaments (K_d > 20 μM; Lee et al., 2000). Because both GST-Myo1p-23 and GST-Myo1p-3A bound verprolin, the SH3 domain mediates this interaction as in budding yeast (Anderson et al., 1998). The affinity of verprolin for actin monomers (K_d ~1 μM) was similar to other proteins with WH2 domains (Hufner et al., 2001; Marchand et al., 2001; Martinez-Quiles et al., 2001; Hertzog et al., 2002).

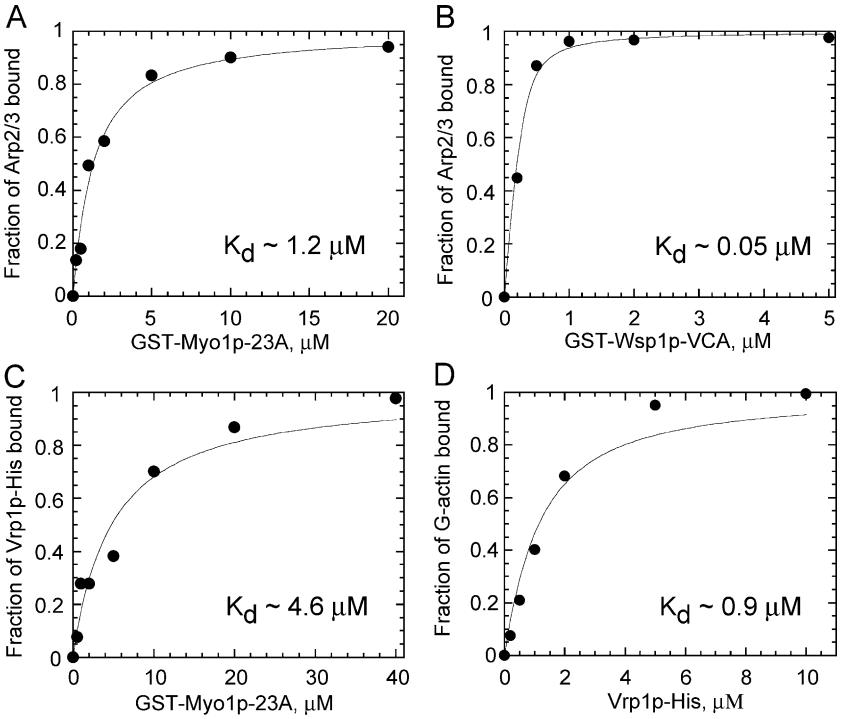

Figure 2. **Interactions among *S. pombe* GST-Myo1p-23A, GST-Wsp1p-VCA, Arp2/3 complex, Vrp1p-His, and actin monomers.** Soluble protein ligands were incubated with a range of concentrations of GST-Myo1p-23A or GST-Wsp1p-VCA immobilized on glutathione-Sepharose or Vrp1p-His bound to Ni-NTA resin. Beads and bound ligand were pelleted and concentrations of bound ligands calculated from measurements of unbound ligands in the supernatants by SDS-PAGE, staining with Coomassie blue and densitometry. (A and B) Binding of 0.3 μM Arp2/3 complex to (A) GST-Myo1p-23A or (B) GST-Wsp1p-VCA immobilized on glutathione beads. (C) Binding of 0.5 μM Vrp1p-His to immobilized GST-Myo1p-23A. Conditions (A–C): 10 mM imidazole, pH 7.0, 50 mM KCl, 1 mM $MgCl_2$, 1 mM EGTA, 0.1 mM ATP, and 1 mM DTT. (D) Binding of 0.5 μM actin monomers to Vrp1p-His immobilized on beads. Conditions (D): 2 mM Tris-HCl, pH 8.0, 0.2 mM ATP, and 0.1 mM $CaCl_2$. Equilibrium dissociation constants were determined by fitting data to binding isotherms (solid lines).

Activation of Arp2/3 complex by Myo1p, Wsp1p, and Vrp1p

We compared the ability of COOH-terminal fragments of Myo1p and Wsp1p each fused to GST to activate Arp2/3 complex. Purified *S. pombe* Arp2/3 complex had little effect on the spontaneous assembly of purified actin monomers (Fig. 3 A). GST-Wsp1p-VCA and GST-Myo1p-23A each activated Arp2/3 complex, resulting in nucleation of new filaments and acceleration of polymerization. Neither GST-Myo1p-23A nor GST-Wsp1p-VCA stimulated actin polymerization in the absence of Arp2/3 complex. GST-Wsp1p-VCA produced three times more actin filament barbed ends than GST-Myo1p-23A (Fig. 3 B). GST-Myo1p-23A did not increase Arp2/3 complex activation by GST-Wsp1p-VCA, so the two activators do not act synergistically (Fig. S1; available at http://www.jcb.org/cgi/content/full/jcb.200502053/DC1). Verprolin did not enhance the ability of GST-Wsp1p-VCA to stimulate actin polymerization by Arp2/3 complex (Fig. 3 A).

Full-length verprolin enhanced the ability of GST-Myo1p-23A to stimulate actin polymerization by Arp2/3 complex (Fig. 3 A). At a concentration (50 nM) of GST-Myo1p-23A that barely activated Arp2/3 complex, Vrp1p produced barbed ends in proportion to its concentration up to 1 μM. Verprolin alone did not activate Arp2/3 complex or stimulate actin polymerization, except for slight increase of rate late in reaction. Verprolin and GST-Myo1p-23A did not stimulate actin assembly without Arp2/3 complex. With a high concentration (500 nM) of verprolin and nanomolar Arp2/3 complex, GST-Myo1p-23A induced formation of five times more barbed ends than in the absence of verprolin (Fig. 3 B), similar to GST-N-WASP-VVCA, the strongest activator described to date (Zalevsky et al., 2001). This corresponds to about one barbed end for every three Arp2/3 complexes. In both the presence and absence of verprolin, the concentration of Myo1p tail required to achieve half-maximal yield of barbed ends was 150 nM, 10-fold higher than GST-Wsp1p-VCA or GST-N-WASP-VVCA (Fig. 3 B). Pre-existing filaments reduced the lag in the actin nucleation by Arp2/3 complex activated by Myo1p tail both in the presence and the absence of verprolin (Fig. 3 C).

The ability of Myo1p tail to activate Arp2/3 complex depended upon both the TH2 and A domains, both in the presence and the absence of verprolin (Fig. S1). In fact, GST-Myo1p-23 lacking the A domain inhibited Arp2/3 complex activation by GST-Myo1p-23A, reducing the number of actin filaments nucleated by Arp2/3 complex by 97% (Fig. 3 D). Verprolin partially overcame this inhibition, resulting in only a 63% decrease in the number of filaments nucleated by Arp2/3 complex. GST-Myo1p-3A tail construct lacking the TH2 domain reduced activation of Arp2/3 complex by GST-Myo1p-23A by 50% without verprolin and 18% with verprolin (Fig. 3 D). Neither GST-Myo1p-23 nor GST-Myo1p-3A inhibited Arp2/3 complex activation by GST-Wsp1p-VCA or assembly of actin alone (Fig. S1).

Arp2/3 complex produced many more branches when activated by GST-Wsp1p-VCA or GST-N-WASP-VVCA than GST-Myo1p-23A with or without verprolin (Fig. 4). Activation of Arp2/3 complex by Myo1p-tail ± verprolin produced only 3–7% filaments with branches, and these rare filaments had but single branches (Fig. 4, B and C). In contrast, 25% of the filaments produced by GST-Wsp1p-VCA and 34% of the filaments produced by GST-N-WASP-VVCA were branched, often with two or more branches (Fig. 4, E and F). The mean lengths of actin filaments in these micrographs agreed with those expected from the concentrations of actin polymer and filament ends calculated from the time course of polymerization (Fig. 4 A).

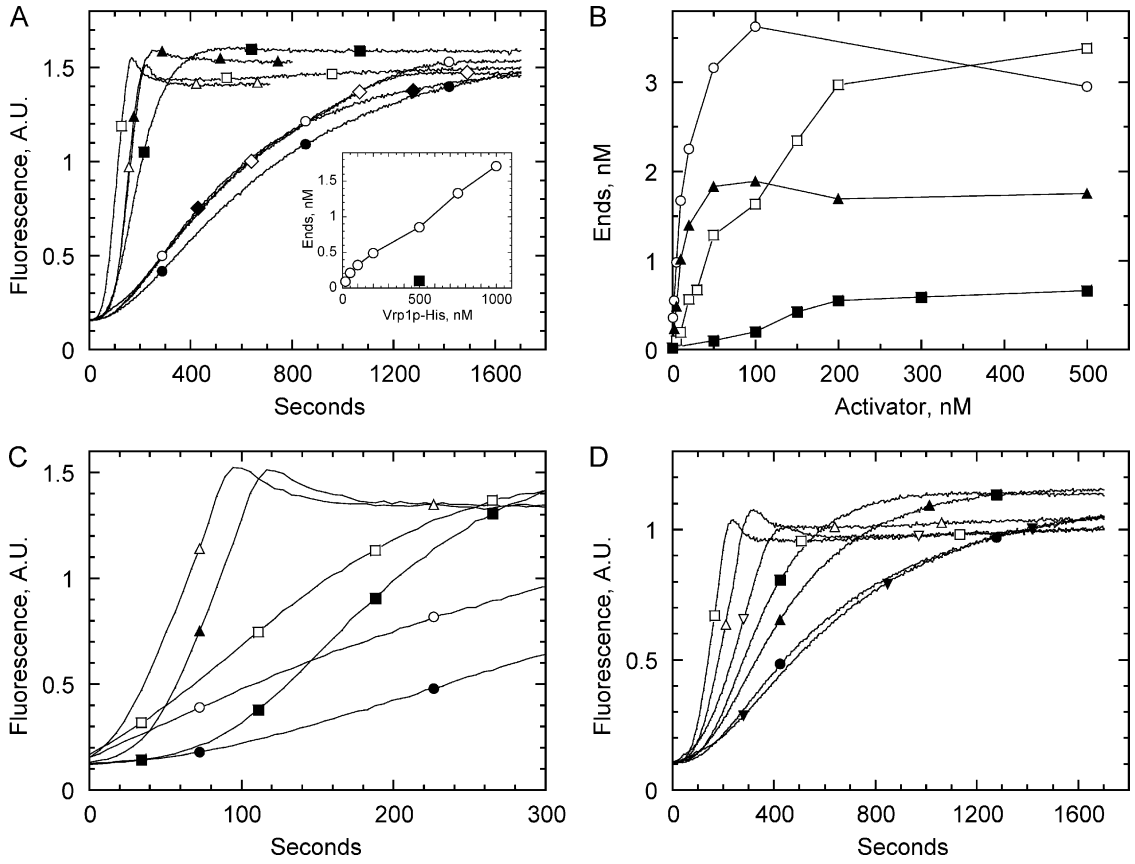

Figure 3. **Actin polymerization assays for the activation of *S. pombe* Arp2/3 complex by WASP-family VCA segments, *S. pombe* Myo1p tail, and verprolin.** Polymerization of 4 μM Mg-ATP actin (5% pyrene-labeled) alone or with 10 nM Arp2/3 complex and activator proteins was measured by the fluorescence of pyrene-labeled actin. Conditions: 10 mM imidazole, pH 7.0, 50 mM KCl, (A–C) 5 mM or (D) 21 mM NaCl, 1 mM $MgCl_2$, 1 mM EGTA, 0.2 mM ATP, 0.5 mM DTT, 1 mM NaN_3, and 20 μM $CaCl_2$. (A) Time course of polymerization of actin (●) alone or with (○) GST-Myo1p-23A + verprolin, (◆) Arp2/3 complex, (◇) Arp2/3 complex + verprolin, (■) Arp2/3 complex + GST-Myo1p-23A, (□) Arp2/3 complex + GST-Myo1p-23A + verprolin, (▲) Arp2/3 complex + GST-Wsp1p-VCA, (△) Arp2/3 complex + GST-Wsp1p-VCA + verprolin at the following concentrations: 200 nM GST-Myo1p-23A, 50 nM GST-Wsp1p-VCA, 100 nM verprolin. Inset: (○) Concentration of actin filament ends generated by 10 nM Arp2/3 complex and 50 nM GST-Myo1p-23A as a function of the concentration of verprolin; (■) reaction without GST-Myo1p-23A. (B) Dependence of the concentration of actin filament ends generated by 10 nM Arp2/3 complex on the concentrations of (■) GST-Myo1p-23A, (□) GST-Myo1p-23A with 500 nM Vrp1p, (▲) GST-Wsp1p-VCA and (○) bovine GST-N-WASP-VVCA. Concentrations of ends were calculated from the polymerization rate when half of the actin was polymerized. (C) Effect of preexisting actin filaments on the time course of actin polymerization stimulated by 10 nM Arp2/3 complex and 200 nM GST-Myo1p-23A alone or with 200 nM verprolin. Buffer or 0.2 μM F-actin were added at the onset of polymerization reactions: actin with (●) buffer or (○) F-actin added to actin alone, (■) buffer or (□) F-actin added to Arp2/3 complex + GST-Myo1p-23A, (▲) buffer (△) or F-actin added to Arp2/3 complex + GST-Myo1p-23A + verprolin. (D) Myo1p tail constructs lacking either the TH2 or A domain inhibit actin polymerization stimulated by 10 nM Arp2/3 complex and 200 nM GST-Myo1p-23A in both the absence and presence of 700 nM verprolin. 1 μM GST-Myo1p-3A or GST-Myo1p-23 was added before reaction onset. Reactions contained (●) actin alone or actin with (■) buffer, (▲) GST-Myo1p-3A, or (▼) GST-Myo1p-23 added to Arp2/3 complex + GST-Myo1p-23A; or actin with (□) buffer, (△) GST-Myo1p-3A, (▽) GST-Myo1p-23 added to Arp2/3 complex + GST-Myo1p-23A + verprolin before reaction onset.

Deletions and functional fluorescent protein tags of Arp2/3 complex activators

None of the three *S. pombe* genes for factors involved in Arp2/3 complex activation (*wsp1*$^+$, *myo1*$^+$, *vrp1*$^+$) is essential for viability. New *Δmyo1* and *Δwsp1* strains with complete ORF deletions showed defects (salt and temperature sensitivity, slow growth, reduced mating, misshapen cells) similar to the original strains (Lee et al., 2000), except that new *Δwsp1* strain, unlike the original strain, was temperature sensitive. A *Δvrp1* strain grew normally at 25°C without morphological defects, but had growth defects at 18 and 36°C as reported by Carnahan and Gould (2003). We constructed a few *Δwsp1 Δvrp1* strains but failed to generate *Δmyo1 Δvrp1* strains, indicating that *Δmyo1* is synthetically lethal with both *Δvrp1* and *Δwsp1* (Lee et al., 2000; Carnahan and Gould, 2003).

We tagged the three nucleation-promoting factors and Arp2/3 complex with monomeric (m) and nonmonomeric fluorescent proteins (GFP, YFP, or CFP) directly in the genome so native promoters controlled expression and cells depended entirely on these fusion proteins. We checked the tagged strains for defects like those observed when these genes are deleted. Cells depending on ARPC5-monomeric GFP (ARPC5-mGFP) grew normally providing that mGFP was separated from ARPC5 by a 6-aa linker. Cells depending on mGFP-Myo1p, mGFP-Wsp1p, or Vrp1p-GFP grew normally, without sensitivity to salt or temperature. mGFP-Myo1p was not synthetically lethal with *Δwsp1* or *Δvrp1* and Vrp1p-GFP was not syntheti-

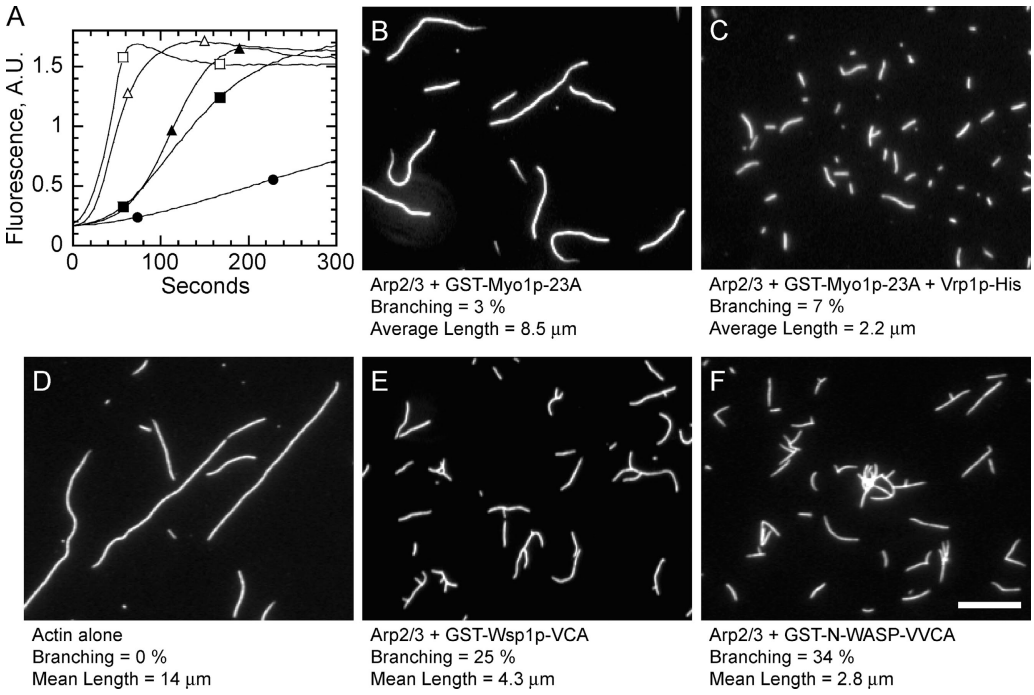

Figure 4. **Fluorescence microscopy of the products of actin polymerization reactions.** Conditions: 4 μM monomeric actin (5% pyrene), 10 mM imidazole, pH 7.0, 50 mM KCl, 5 mM NaCl, 1 mM $MgCl_2$, 1 mM EGTA, 0.2 mM ATP, 0.5 mM DTT, 1 mM NaN_3, and 20 μM $CaCl_2$. After mixing the reactants, the samples were split into two: (A) pyrene fluorescence was used to monitor the polymerization of one aliquot; (B–F) 4 μM rhodamine-phalloidin was added to the other aliquot. When each reaction was 80% complete, the aliquot with rhodamine-phalloidin was diluted 400 times into microscopy buffer (10 mM imidazole, pH 7.0, 50 mM KCl, 1 mM $MgCl_2$, 100 mM DTT, 20 μg/ml catalase, 100 μg/ml glucose oxidase, 3 mg/ml glucose, and 0.5% methylcellulose) and 2 μl were applied to the nitrocellulose-coated 22 × 22-mm coverslip. (A) Time course of polymerization and (D–F) micrographs of rhodamine-phalloidin stained actin filaments from polymerization reactions: (D, ● in A) actin alone at 1,000 s, or actin with (B, ■ in A) 10 nM Arp2/3 complex with 900 nM GST-Myo1p-23A at 200 s, (C, □ in A) 10 nM Arp2/3 complex with 900 nM GST-Myo1p-23A and 500 nM Vrp1p-His at 60 s, (E, ▲ in A) 10 nM Arp2/3 complex with 500 nM GST-Wsp1p-VCA at 150 s, (F, △ in A) 10 nM Arp2/3 complex with 500 nM GST-N-WASP-VVCA at 80 s. Bar, 10 μm.

cally lethal with *Δmyo1*. In contrast, we were unable to generate an *mGFP-wsp1 Δmyo1* strain by genetic crosses. Because the time course of patch assembly appears entirely normal in strains depending on mGFP-Wsp1p (see further), inability to generate a *mGFP-wsp1 Δmyo1* strain by genetic crosses may be due to mGFP-Wsp1p failing to function during mating, sporulation, or spore germination.

Localization of Arp2/3 complex and activators in dynamic actin patches

We used spinning disk confocal microscopy to localize Arp2/3 complex and mGFP-Myo1p, mGFP-Wsp1p, and Vrp1p-GFP in cortical patches of live yeast cells (Fig. S2, available at http://www.jcb.org/cgi/content/full/jcb.200502053/DC1). The signal from ARPC5-mGFP was the strongest, followed by mGFP-Myo1p, mGFP-Wsp1p, and the Vrp1p-GFP. All three activators had similar lifetimes (Table S1, available at http://www.jcb.org/cgi/content/full/jcb.200502053/DC1) of 10 (±3) seconds (range 6 to 18 s). In 3D reconstructions, mGFP-Myo1p fluorescence also faintly outlined the entire cell cortex, and mGFP-Wsp1p also had a high level of cytoplasmic fluorescence. The mGFP-Myo1p patches were stationary in time-lapse movies of Z-series of optical sections through entire cells, whereas some mGFP-Wsp1p and Vrp1p-GFP patches moved centripetally during the last 3 s of their lifetimes. ARPC5-mGFP localized to motile patches with average lifetimes of 22 s. ARPC5-mGFP patches were stationary during the first half of their lifetimes, as they formed in the cell cortex. Then they moved centripetally 0.4–2 μm over an average of 10 s before fading (Fig. S2). Disruption of actin filaments with 100 μM latrunculin A eliminated dynamic activator patches and resulted in clumping of mGFP-Wsp1p, Vrp1p-GFP, and occasionally mGFP-Myo1p at the ends of the cells (Fig. S2).

Z-series through entire cells expressing all combinations of pairs of the three activators tagged with YFP/CFP showed all three proteins localized in the same patches (Fig. 5; Table S2, available at http://www.jcb.org/cgi/content/full/jcb.200502053/DC1). mCFP-Wsp1p and Vrp1p-YFP fluorescence closely overlapped in 87% of patches. 80% of patches contained both mCFP-Myo1p and mYFP-Wsp1p and 78% contained mCFP-Myo1p and Vrp1p-YFP. The remaining ∼20% of patches contained only one of the two fluorescently labeled activators, indicating differences in timing of patch assembly among activators. Patches of Myo1p appeared to be more spread out along the membrane than Wsp1p and Vrp1p by 1–2 pixels (100–200 nm).

Z-series through entire cells expressing pairs of patch proteins revealed that 65–75% of patches of Arp2/3 complex labeled with mCFP included activator proteins labeled with mYFP or YFP (Fig. 5, Table S2). Remaining patches either had the activator alone or Arp2/3 complex alone. A higher fraction of patches appeared to have both an activator and Arp2/3 complex when activators were tagged with CFP and Arp2/3 complex with YFP, owing to the weaker signal from CFP than

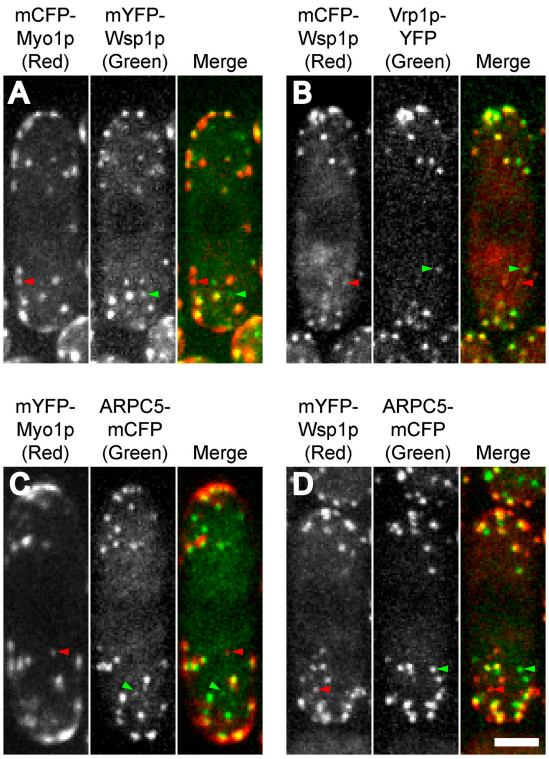

Figure 5. **Localization of Myo1p, Wsp1p, Vrp1p, and Arp2/3 complex (ARPC5) by fluorescence microscopy of live cells expressing pairs of proteins tagged with YFP and CFP.** Each panel is a maximum projection image of a stack of spinning disk confocal sections taken at 0.6-μm intervals. (A) mCFP-Myo1p (red) and mYFP-Wsp1p (green). (B) mCFP-Wsp1p (red) and Vrp1p-YFP (green). (C) mYFP-Myo1p (red) and ARPC5-mCFP (green). (D) mYFP-Wsp1p (red) and ARPC5-mCFP (green). The same color code is used for arrowheads that point out examples of patches labeled only with CFP or YFP. Yellow indicates colocalization in the merged images. Bar, 2 μm.

YFP, especially at the initial stages of patch assembly. In all cases, the Arp2/3 complex fluorescence overlapped only partially with the activator fluorescence, with Arp2/3 complex deeper inside the cell than the activators.

Time course of patch assembly

We determined the time course of patch formation, maturation, and dissolution by time-lapse microscopy of cells expressing an activator tagged with mYFP and Arp2/3 complex tagged with mCFP (Fig. 6, Videos 1 and 2). A time series in a single confocal plane (Fig. 7, A–D) showed that mYFP-Myo1p concentrated in a stationary patch 3 s before a spatially coincident ARPC5-mCFP signal appeared and then increased in intensity over the next 6–9 s. At this point the mYFP-Myo1p fluorescence began to decline and the ARPC5-mCFP signal moved away from the membrane for another 9–12 s. Tracking patches in 3D movies (Fig. S2, Table S1) showed that ARPC5-mGFP behaved similarly to ARPC5-mCFP in 2D, indicating that patches remained visible in single confocal mid-sections throughout the span of their movements. Arp2/3 complex patches moved for 400–1,800 nm (average, 800 nm) with velocities ranging from 30 to 230 nm/s (average, 90 nm/s). The behavior of patches marked with mYFP-Wsp1p and ARPC5-mCFP was similar (Fig. 6, E–G), although ARPC5 arrived 6 s after Wsp1p. The same was true for patches marked with Vrp1p-YFP and ARPC5-mCFP (Fig. 6, H–J). Thus, Wsp1p/Vrp1p arrive in patches ~3 s before Myo1p.

The onset of the activator patch disassembly always coincided with initiation of Arp2/3 complex movement. During rapid disassembly of the activator patches, mYFP-Myo1p remained stationary in the cell cortex for ~6 s, whereas mYFP-Wsp1p and Vrp1p-YFP moved along with Arp2/3 complex for ~3 s and 100–400 nm and then disappeared (Fig. 6, G and J). Thus, Wsp1p/Vrp1p disappeared ~3 s before Myo1p. The difference in timing of Myo1p and Wsp1p/Vrp1p arrival in patches explains the differences in the number of activator-only patches observed by colocalization at a single time point (Fig. 5). When activators were labeled with YFP and Arp2/3 complex with CFP, the fraction of patches with Wsp1p alone (23%) or Vrp1p alone (15%) was higher than Myo1p alone (8%). Wsp1p and Vrp1p arrive earlier than Myo1p, and therefore spend a smaller fraction of their lifetime associated with Arp2/3 complex patches. The lifetimes of YFP-labeled activator patches observed in single confocal sections were 6–9 s longer than lifetimes of GFP-labeled patches in 3D movies (Table S1). This is likely due to the faint signals when short exposure times were used to minimize photobleaching of GFP during 4D data collection.

Time course and genetic dependence of activator patch assembly

To observe directly the timing of activator assembly/disassembly in patches, we made movies of cells expressing pairs of activators tagged with YFP and CFP. Wsp1p and Vrp1p arrived at the site of patch assembly slightly before Myo1p, and Myo1p persisted longer than Wsp1p. In time series taken at 3-s intervals, mYFP-Wsp1p appeared 3–6 s and disappeared 3 s before mCFP-Myo1p (Fig. 7, A and B). Activators remained together in patches for 9–12 s. After that, Wsp1p and Vrp1p moved together a short distance into the cytoplasm for ~3 s while Myo1p remained in the cortical patch, persisting on average for ~3 s after Wsp1p disappeared. The time courses of concentration of Myo1p, Wsp1p, and Vrp1p at patches explain the existence of patches with Myo1p or Wsp1p alone. The timings observed for activator pairs were consistent with movies of each activator paired with Arp2/3 complex (Fig. 6).

Strains lacking one of the activators showed that Myo1p and Wsp1p arrive at patches independently, and that Wsp1p, but not Myo1p, is required to bring Vrp1p to patches. We made five double strains by crossing mGFP-Myo1p, mGFP-Wsp1p, and Vrp1p-GFP strains with *Δmyo1*, *Δwsp1*, and *Δvrp1* strains (Fig. 7, C–H; Table S1). Immunoblots showed that none of the gene deletions altered the abundance of other GFP-tagged activators more than 30%. The localization and dynamics of mGFP-Myo1p and mGFP-Wsp1p in cortical patches was indistinguishable in *vrp1*$^+$ and *Δvrp1* cells, but no Vrp1p-GFP patches formed in *Δwsp1* cells. mGFP-Myo1p concentrated in dynamic cortical patches in *Δwsp1* cells, but the lifetimes of these patches were almost twice that in *wsp1*$^+$ cells. Vrp1p-GFP formed dim dynamic cortical patches (presumably containing Wsp1p) in *Δmyo1* cells; however, these patches were abnormal: up to half formed and faded repeat-

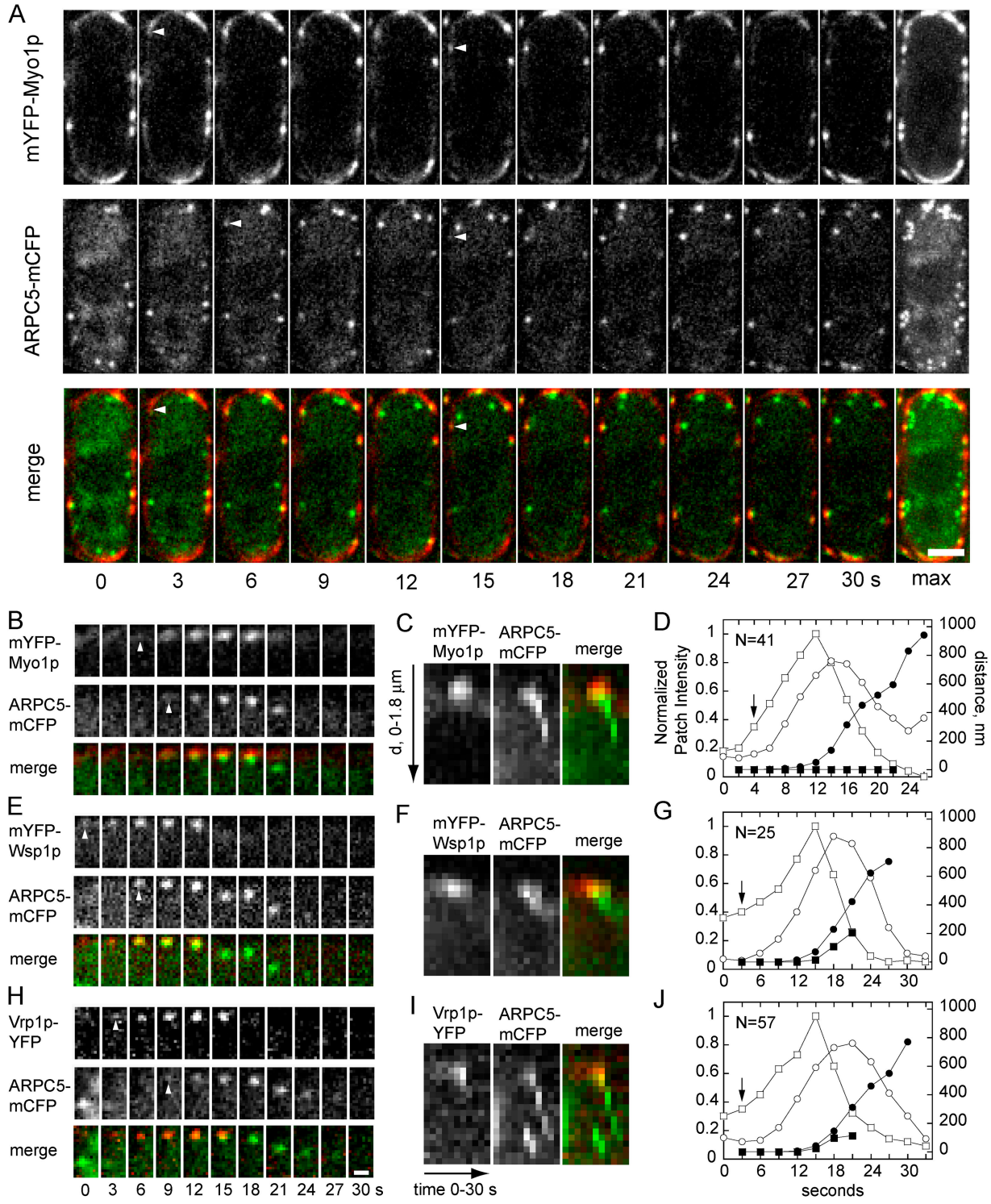

Figure 6. **Dynamics of activator patches and Arp2/3 complex patches in live cells expressing pairs of fluorescent fusion proteins.** Activators (Myo1p, Wsp1p, Vrp1p) are red and Arp2/3 complex (ARPC5) is green in color images. (A) Time series of mYFP-Myo1p (red) and ARPC5-mCFP (green) in a single confocal plane at 3-s intervals. The "max" frame is a maximum projection image of the entire time series. Bar, 2 µm. (B–J) Quantitative analysis of patch dynamics. (B–D) mYFP-Myo1p and ARPC5-mCFP. (E–G) mYFP-Wsp1p and ARPC5-mCFP. (H–J) Vrp1p-YFP and ARPC5-mCFP. (B, E, and H) Time courses of individual patches at 3-s intervals in a single optical plane. Bar, 0.5 µm. (C, F, and I) Kymographs of individual patches. At 3-s intervals a 20 × 10-pixel box was maximally projected onto a 20 × 1-pixel vertical lane. Eleven such lanes were combined horizontally to generate kymographs. (D, G, and J) Time courses of average intensity of (□) activators and (○) Arp2/3 complex and total distance moved by (■) activators and (●) Arp2/3 complex in 20–60 individual patches tracked in a single optical plane at intervals of (D) 2 s or (G and J) 3 s. Fluorescence intensity values were normalized, data from individual patches were aligned to the peak of activator patch (YFP) intensity for calculation of average normalized intensity and position. In all panels arrows and arrowheads mark initiation of activator or Arp2/3 complex patch assembly.

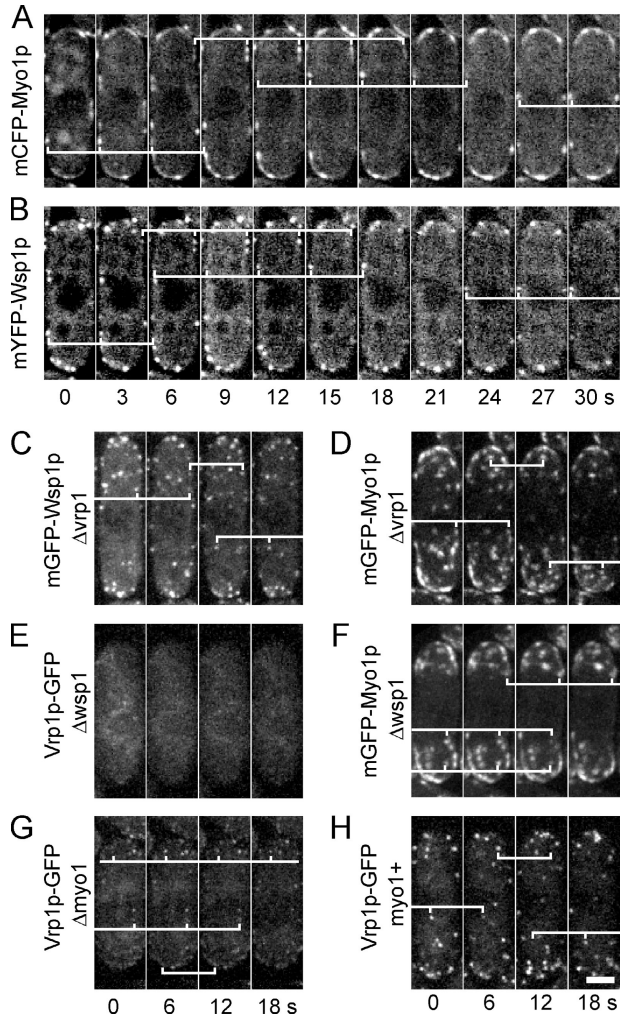

Figure 7. **Time course and genetic dependencies of activator patch assembly.** (A and B) Images from single confocal planes at 3-s intervals of a cell expressing mCFP-Myo1p and mYFP-Wsp1p. White brackets highlight several corresponding YFP- and CFP-labeled patches. Appearance of mCFP lags behind mYFP-Wsp1p by 3–6 s. (C–H) Assembly of activators tagged with GFP in strains with genetic deletions of other activators. GFP-tagged activators were combined with deletions by genetic crosses. Maximum projection images of Z-series at 6-s intervals. (C) mGFP-Wsp1p in *Δvrp1*. (D) mGFP-Myo1p in *Δvrp1*. (E) Vrp1p-GFP in *Δwsp1*. (F) mGFP-Myo1p in *Δwsp1*. (G) Vrp1p-GFP in *Δmyo1*. (H) Vrp1p-GFP patches in *myo1*$^{+}$ are brighter than in *Δmyo1* (G). White brackets mark patches throughout their lifetimes. Bar, 2 μm.

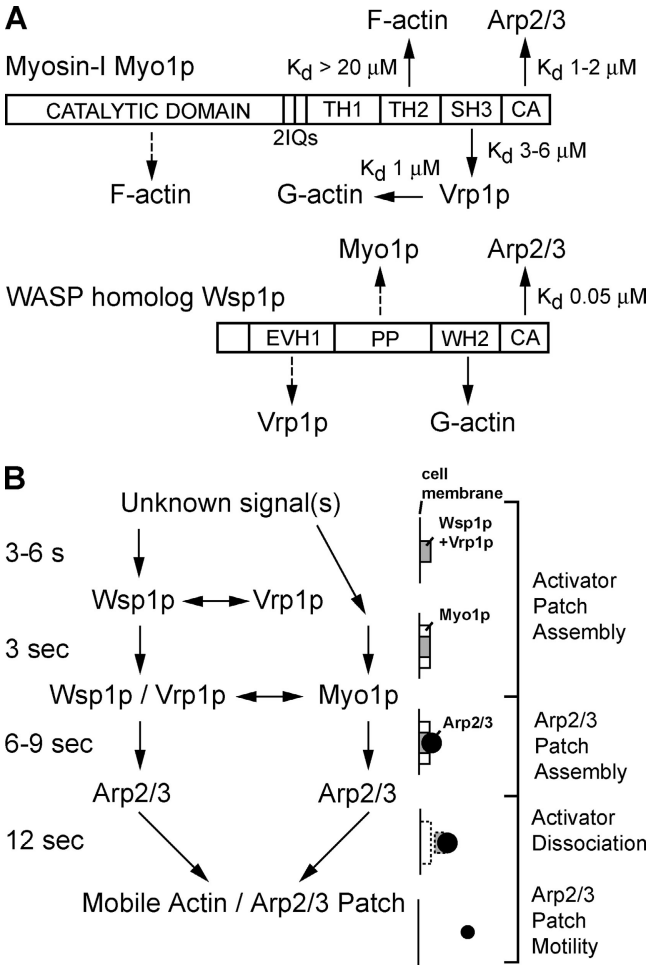

Figure 8. **Summary of biochemical interactions and timing of patch assembly of Myo1p, Wsp1p, Vrp1p, and Arp2/3 complex in *S. pombe*.** (A) Schematic diagrams of biochemical interactions among Myo1p, Wsp1p, Vrp1p, Arp2/3 complex, and actin. Solid lines indicate interactions demonstrated in vitro in this study. Dashed lines indicate putative interactions based on studies in budding yeast. (B) Proposed pathway of actin patch assembly. Patch formation is divided into three phases: (1) activator patch assembly, (2) Arp2/3 complex patch assembly, and (3) Arp2/3 complex patch motility. (1) Activator patch assembly starts with aggregation of Wsp1p associated with Vrp1p into a nascent patch followed by Myo1p 3–6 s later. Wsp1p/Vrp1p and Myo1p assemble into the same patch independently but may interact in the patch, influencing patch dynamics. (2) Arp2/3 complex begins to assemble into a patch 3 s after Myo1p arrives. At this stage the Arp2/3 complex patch is immobile and closely associated with the activator patch for 6–9 s. (3) Arp2/3 complex patch initiates movement away from cell membrane as activator patch disassembles. During disassembly Wsp1p and Vrp1p follow Arp2/3 complex away from the membrane while Myo1p remains behind. Activator patch disassembles in 3–6 s and Arp2/3 complex patch moves for 9–12 s.

edly at the same site; some persisted over 20 s; and others were short-lived, with lifetimes of only 6 s.

Discussion

Two parallel pathways of yeast actin patch assembly

Biochemical analysis, time-lapse imaging of fluorescent fusion proteins, and genetic dependencies gave a consistent picture of actin patch formation, consisting of three phases (Fig. 8). Phase 1 begins with Wsp1p recruiting Vrp1p to a small patch near the inner surface of the plasma membrane over 3–6 s. Then, Myo1p joins this patch over the next 3 s. Myo1p localization requires actin filaments, but not Wsp1p or Vrp1p. Phase 2 starts with the arrival of Arp2/3 complex 3 s after Myo1p. Over the next 6–9 s, the concentrations of three activators and Arp2/3 complex steadily increase in the stationary patch. At phase 3, as the concentrations of all four proteins peak, the Arp2/3 complex patch begins to move toward cell interior at 30–230 nm/s. Myo1p stays behind and disappears in 6 s. Wsp1p and Vrp1p move a short distance with Arp2/3 complex but dissipate in 3 s. Arp2/3 complex moves 0.4–1.8 μm over 9–12 s while gradually fading.

The key feature of the actin patch assembly is that it proceeds through parallel Wsp1p and Myo1p pathways that both converge on Arp2/3 complex (Fig. 8). In vitro Wsp1p and Myo1p activate Arp2/3 complex independently, and in vivo either pathway is sufficient for patch assembly and cell viability (Lee et al., 2000). Localization and genetic analysis place verprolin in the Wsp1p pathway. However, physical interactions among activators, including Vrp1 binding to Myo1p, may bridge the two pathways.

Budding yeast also has parallel pathways to Arp2/3 complex dependent on myosin-I and WASp (Evangelista et al., 2000; Lechler et al., 2000, 2001; Kaksonen et al., 2003; Jonsdottir and Li, 2004). Budding yeast WASp Las17p/Bee1p localizes to patches before myosin-I Myo5p and actin polymerization begins after Myo5p arrival (Kaksonen et al., 2003; Jonsdottir and Li, 2004). Upon full assembly of actin and dissociation of activators, actin patches move over 500 nm with velocities of 200–400 nm/s (Waddle et al., 1996; Smith et al., 2001; Kaksonen et al., 2003), similar to Arp2/3 complex patches in fission yeast.

On the other hand, patch assembly differs both qualitatively and quantitatively in the two yeast. First, the lifetime of Las17p/Bee1p patches (40 s) (Kaksonen et al., 2003) is significantly longer than fission yeast Wsp1p patches (10–17 s). Class 1 myosin patches (Jonsdottir and Li, 2004) have similar lifetimes in both yeast (10–20 s). Second, actin patches move slowly (25 nm/s) over a short distance (200 nm) before initiating fast long-range motility in budding yeast (Kaksonen et al., 2003) but not fission yeast. Third, deletion of budding yeast *VRP1* depolarizes actin patches, whereas patches remain polarized in fission yeast *Δvrp1*. As a result, budding yeast *Δvrp1* cells have severe endocytic and actin cytoskeletal defects (Donnelly et al., 1993; Munn et al., 1995; Vaduva et al., 1997), like *Δlas17* cells (Li, 1997), whereas fission yeast without Vrp1p have no apparent defects at 25°C (this paper).

Wsp1p-dependent pathway of actin assembly

Fission yeast WASp homologue Wsp1p is the first nucleation-promoting factor to assemble into a patch. Like other WASp/WAVE family members (Higgs and Pollard, 2001), *S. pombe* GST-Wsp1p-VCA activates *S. pombe* Arp2/3 complex to nucleate branched actin filaments. GST-Wsp1p-VCA is less active than GST-N-WASP-VVCA, keeping with the trend that strength of nucleation-promoting factors is proportional to the number of acidic residues in the A-domain (Zalevsky et al., 2001). Wsp1p has 10 acidic residues compared with 18 for neuronal WASp (N-WASP).

Recruitment of Vrp1p to patches depends on the presence of Wsp1p, and the two proteins remain together throughout the life of a patch. The close association of WASp and verprolin in budding yeast and vertebrates (Lechler et al., 2001; Ho et al., 2004) is mediated through interaction of a conserved Ena/VASP homology 1 domain of WASp with a proline-rich sequence in the COOH-terminal half of verprolin (Ramesh et al., 1997; Naqvi et al., 1998; Volkman et al., 2002). WASp-interacting protein has been suggested to inhibit N-WASP (Martinez-Quiles et al., 2001; Ho et al., 2004), but this seems unlikely in *S. pombe* because activator and actin patches are normal in *Δvrp1* cells.

Myo1p-dependent pathway of actin assembly

Myo1p localizes in patches independently of Wsp1p or Vrp1p. The tail of Myo1p weakly activates actin nucleation of unstable branches by Arp2/3 complex. The low activity may be related to the 20-fold lower affinity of Myo1p tail for Arp2/3 complex than Wsp1p-VCA. Accordingly, 10-fold more Myo1p tail is required to make half the number of filaments as Wsp1p-VCA. Verprolin strongly stimulates the activity of Myo1p tail, but does not reduce the concentration of Myo1p tail required for half-maximal activation. The ability of preformed filaments to reduce the lag phase of actin nucleation by Arp2/3 complex stimulated by Myo1p tail is evidence that nucleation involves binding of Arp2/3 complex to preexisting filaments, even though most of these branches dissociate before growing long enough to be detected by microscopy.

Myo1p and Wsp1p/Vrp1p cooperate in patch assembly

Cellular experiments suggest that patch assembly depends on coordination of the Wsp1p/Vrp1p and Myo1p pathways to Arp2/3 complex. Cells lacking either Myo1p or Wsp1p have depolarized actin patches and severe defects in growth, morphology, septation, and mating (Lee et al., 2000). Myo1p patches in *Δwsp1* and Vrp1p patches in *Δmyo1* are abnormal. Thus, Myo1p and Wsp1p/Vrp1p are recruited separately but cooperate in patch assembly by direct physical interaction or providing complementary biochemical activities.

Vrp1p strongly enhances the ability of Myo1p tail to activate Arp2/3 complex. High concentrations are required, owing to the low affinity of Vrp1p for Myo1p tail (K_d 3–6 μM). Vrp1p may provide a WH2 domain to complement the A domain provided by Myo1p, forming a complete VCA nucleation-promoting factor (Evangelista et al., 2000; Lechler et al., 2000; Machesky, 2000). Budding yeast Vrp1p WH2 domain can substitute for native WH2 in GST-Las17p-VCA (Lechler et al., 2001).

On the other hand, the available assays have detected no impact of the absence of Vrp1p on fission yeast actin patches. Although this observation does not rule out the possibility that Vrp1p stimulates Myo1p when concentrated in the patch, it suggests that other factors may bridge the two pathways. Conversely, each pathway may contribute nonredundant biochemical activities. Activation of Arp2/3 complex by Myo1p and Wsp1p/Vrp1p in vitro is not cooperative. As a stronger activator, Wsp1 may be the primary activator, whereas affinity of the motor domain of full-length Myo1p for actin filaments may also contribute to assembling activated Arp2/3 complex (Lechler et al., 2000, 2001), perhaps by capturing and tethering actin filaments and/or cables. Myo1p may also help to retain Vrp1p and Wsp1p in the patch, consistent with the observation that Vrp1p patches in *Δmyo1* are dim and show abnormal dynamics, similar to actin patches in budding yeast lacking type 1 myosins (Smith et al.,

2001; Rodal et al., 2005). Alternatively, two pathways may link different upstream signals to actin assembly.

Functions of yeast actin patches

Mounting evidence in budding yeast indicates that actin patches form at the sites of endocytosis (Kaksonen et al., 2003; Huckaba et al., 2004; Jonsdottir and Li, 2004), so we presume that fission yeast actin patches do as well. The fission yeast genome has homologues of the genes for all the budding yeast endocytic/actin cytoskeletal adaptor proteins that assemble into a nascent actin patch before Arp2/3 complex (Kaksonen et al., 2003). For example, deletion or depletion of the homologues *SLA2* in budding yeast (Kaksonen et al., 2003), Hip1R in cultured cells (Engqvist-Goldstein et al., 2004), or *end4*$^{+}$ in *S. pombe* (Iwaki et al., 2004) cause endocytic defects.

Electron micrographs show budding yeast actin patches associated with membrane invaginations and vesicles (Mulholland et al., 1994; Jonsdottir and Li, 2004; Young et al., 2004; Rodal et al., 2005). Actin patches purified from budding yeast contain a network of short (50 nm) branched filaments, as expected for assembly driven by Arp2/3 complex (Young et al., 2004). Based on orientation of filaments in actin comet tails in budding yeast *Δsla2*, Kaksonen et al. (2003) proposed that filament barbed ends push against the plasma membrane. This is consistent with the localization of Arp2/3 complex and actin observed by Rodal et al. (2005).

Fission yeast have structures called filasomes, 300-nm clouds of actin filaments surrounding vesicles 35–70 nm in diameter (Takagi et al., 2003). Filasomes were proposed to be exocytic vesicles, but they may actually be actin patches associated with endocytosis. If so, then 300 nm is the maximum length filaments grow in 6 s of patch assembly. That corresponds to elongation at a rate of ~20 subunits per second and free G-actin concentration of 2 μM. This may be an underestimate, as each filament may grow for <6 s, owing to termination by capping protein.

Actin assembly at the neck of an endocytic vesicle is proposed to assist in either pinching off or propelling the vesicle away from plasma membrane (Munn, 2001; Engqvist-Goldstein and Drubin, 2003; Merrifield, 2004). Fission yeast patches are stationary as they assemble and initiate motility only when fully grown. This is consistent with the idea that patches move after actin assembly severs the vesicle from the plasma membrane (Kaksonen et al., 2003).

Actin polymerization may drive short local movements of actin patches, but long-range movements seem to depend on association with moving actin cables in both fission (Pelham and Chang, 2001) and budding yeast (Huckaba et al., 2004). The brief (~20 s) lifetime and slow (30–230 nm/s) movements of Arp2/3 complex patches are significantly different from lifetimes of over 30 s and rates of movement of 300 nm/s of actin patches labeled by coronin Crn1p-GFP or App1p-GFP (Pelham and Chang, 2001). We confirmed (unpublished data) that Crn1p-GFP behaves differently from GFP-tagged Arp2/3 complex, capping protein, fimbrin, twinfilin, and actin in that it lacks a distinct stationary phase and has a prolonged mobile phase. Crn1p-GFP may join patches at the onset of mobile phase and remain in the patch longer than other markers.

Actin patches as a model for the leading edge

Live cell imaging of kinetics of activators and Arp2/3 complex during actin patch assembly shows that nucleation-promoting factors associate transiently with Arp2/3 complex. The signal from Arp2/3 complex overlaps for at least 6 s with Myo1p and 6–9 s with Wsp1 before Arp2/3 complex moves away from the activators associated with the plasma membrane. Thus, these nucleation-promoting factors are bound to Arp2/3 complex for no more than 9 s—probably less. Purified VCA activators dissociate rapidly from both actin and Arp2/3 complex (Marchand et al., 2001). Such a transient interaction of ActA with Arp2/3 complex may account for the drag observed between real or artificial bacteria and their actin comet tails (Giardini et al., 2003; Upadhyaya et al., 2003). These events cannot be resolved at the leading edge of motile cells because activation of Arp2/3 complex is continuous and asynchronous. Fortunately, yeast actin patches assemble and disassemble in a "single turnover" reaction that occurs in a strictly defined temporal order. This feature, along with the ease of varying the concentration of any protein at will, make yeast actin patches a simple experimental model for studying reactions relevant to actin assembly in more complex systems, such as the leading edge of motile cells.

Materials and methods

Bacterial expression constructs

For NH_2-terminal GST tagging, DNA inserts encoding Myo1p TH2-SH3-CA, TH2-SH3, and SH3-CA tail fragments, as defined by Lee et al. (2000), or Wsp1p VCA (aa 497–574), bovine N-WASP VCA (aa 422–505), and VVCA (aa 402–505) were subcloned into BamH1 and EcoR1 sites of pGEX-2T and pGEX-6P-1 (GE Healthcare). To add COOH-terminal His-tag, full-length Vrp1p cDNA was subcloned into Nde1 and Xho1 sites of pET21a (Novagen). Myo1p and N-WASP inserts were PCR amplified using Turbo Pfu (Stratagene) from pBS-myo1 (Lee et al., 2000) and N-WASP VVCA in pGEX-2T, respectively. To avoid introns, inserts for Wsp1p and Vrp1p constructs were amplified by RT-PCR (GIBCO BRL) from total *S. pombe* RNA.

Protein purification

Native *S. pombe* Arp2/3 complex was purified from protease-deficient TM011 cells resuspended in buffer U (50 mM Hepes, pH 7.5, 100 mM KCl, 3 mM $MgCl_2$, 1 mM EGTA, 0.1 mM ATP, and 1 mM DTT) containing Complete (Roche) protease inhibitors and ruptured using a Microfluidizer (model M-110S; Microfluidics). After lysates were spun at 100,000 *g*, proteins were precipitated by 50% ammonium sulfate, solubilized in buffer U, and dialyzed against buffer A (50 mM Tris-HCl, pH 7.5, 25 mM KCl, 1 mM $MgCl_2$, 1 mM EGTA, 0.1 mM ATP, and 1 mM DTT) with 0.5 mM PMSF. Arp2/3 complex was bound to GST-N-WASP-VCA immobilized on glutathione-Sepharose, eluted with 1 M NaCl in buffer A, dialyzed against buffer Q (10 mM Pipes, pH 6.8, 0.25 mM $MgCl_2$, 0.25 mM EGTA, and 1 mM DTT), and further purified by ion exchange chromatography on a Source 15Q column (AKTA FPLC; GE Healthcare).

Vrp1p-His was expressed in *Escherichia coli* strain Rosetta (DE3) pLysS (Novagen) at 22°C and purified using Ni-NTA resin (QIAGEN). Eluate from Ni-NTA column was dialyzed against buffer QA (10 mM Tris-HCl, pH 8.0, 1 mM EGTA, and 1 mM DTT), passed over a Source 15Q column, and fractionated on a Source 15Q column. Pure Vrp1p-His eluted in 145 mM NaCl.

GST fusion proteins were purified as described for human WASp GST-VCA (Higgs et al., 1999). GST-tagged Myo1p fragments were stored in buffer QA containing 275 mM NaCl.

Actin polymerization assays

Actin polymerization assays were performed using an Alphascan spectrofluorimeter (Photon Technology International) and analyzed as described previously (Higgs et al., 1999). Products of actin polymerization were

stained with equimolar rhodamine-phalloidin (Fluka) added at the reaction onset as described by Blanchoin et al. (2000). Images were collected on a microscope (model 1X-71; Olympus) equipped with a 60×, 1.4 NA PlanApo lens using an ORCA-ER CCD camera (Hamamatsu Corporation) controlled by MetaMorph (Universal Imaging Corp.).

Quantitative pull-down assays

Equilibrium dissociation constants (K_d) were measured by quantitative pull-down assays (Lee et al., 1999). GST- or His-tagged receptors at variable concentrations [R] were immobilized on beads and incubated with soluble ligand at constant concentration [L]. Concentrations of unbound ligand were measured by gel densitometry and fraction of ligand bound [LR]/[L] was fitted to binding isotherm in KaleidaGraph (Synergy Software): [LR]/[L] = (([R] + [L] + K_d) − (([R] + [L]+K_d)^2 − 4*[R]*[L])^0.5)/2*[L].

Construction of yeast strains

Genes at their chromosomal loci were either deleted or tagged with fluorescent protein (FP) sequences using the PCR-based gene tagging technique (Bahler et al., 1998; Wu et al., 2003). In *Δvrp1*, *Δmyo1*, *Δwsp1* pFA6a-kanMX6 cassette replaced the entire ORFs. Vrp1p was tagged at the COOH terminus with nonmonomeric FPs by integrating pFA6a-GFP(S65T)-kanMX6 cassette and its YFP and CFP derivatives in place of the stop codon. ARPC5 was tagged at the COOH terminus with monomeric FPs containing A206K mutation (Zacharias et al., 2002) and separated from the ARPC5 by GGRGGR linker. Myo1p and Wsp1p were tagged at their NH_2 termini with monomeric FPs and expressed under control of native promoters by replacing *myo1* nt −106 to +47 and *wsp1* nt −112 to +3 with monomeric FP derivatives of pFA6-kanMX6-P3nmt1-GFP in which *nmt1* promoter was replaced with nt −1185 to −1 of *myo1* or nt −512 to −1 of *wsp1*, respectively. Strains combining tags and deletions of two genes were constructed by genetic crosses. To promote mating, *Δmyo1* and *Δwsp1* were transformed with pUR19 containing *myo1*$^+$ and *wsp1*$^+$, respectively (Lee et al., 2000), which were lost upon spore germination. All genomic integrations were confirmed by PCR and microscopy of FPs.

Microscopy

Fluorescence images of live cells on pads of 25% gelatin in EMM2 (Wu et al., 2003) at 21–23°C were captured with an ORCA-ER CCD camera (Hamamatsu Corporation) using the UltraView RS (PerkinElmer) spinning disk confocal system installed on a microscope (model IX-71; Olympus) equipped with a 100×, 1.4 NA PlanApo lens (Olympus). Time series of Z-stacks at 0.6-μm steps were collected for GFP. CFP and YFP were imaged sequentially throughout Z-series for colocalization analysis or time series in a single Z-section for tracking patch dynamics. Image analysis was done in Image J (W. Rasband, National Institutes of Health, Bethesda, MD). Patch lifetimes were estimated visually and patch size was defined by the area with above background fluorescence. Patches were tracked manually using a 600-nm circle centered on each patch. YFP and CFP patches were considered colocalized if their outlines overlapped. Mean fluorescence intensity and position of patches were tracked through time series. Fluorescence intensities were normalized and individual patch data were averaged in Microsoft Excel upon aligning data to the peak of YFP intensity. The results of manual patch tracking were confirmed by fitting patch intensities to parabolic or Gaussian functions using a custom-written Image J plug-in (J. Kuhn, Yale University, New Haven, CT).

Online supplemental material

Video 1 shows a time-lapse movie of mYFP-Myo1p (red) and ARPC5-mCFP (green). Video 2 shows a time-lapse movie of mYFP-Wsp1p (red) and ARPC5-mCFP (green). Fig. S1 shows truncation analysis of Myo1p tail. Fig S2 depicts localization and dynamics of GFP-tagged proteins. Table S1 lists lifetimes of FP-tagged proteins in patches. Table S2 shows colocalization of FP-tagged proteins in patches. Table S3 lists yeast strains. Online supplemental material available at http://www.jcb.org/cgi/content/full/jcb.200502053/DC1.

We are grateful to Drs. T. Toda and M. Yanagida for protease-deficient yeast strain, R. Li for a protocol to purify Arp2/3 complex, W-L. Lee for Myo1p constructs, H. Higgs for N-WASP construct, J. Kuhn for help with image analysis, and S. Forsburg for valuable advice. We thank C. Dillingham and K. Macmillan for help with patch tracking.

This work was supported by National Institutes of Health grants 26132 and 26338 (to T.D. Pollard) and American Heart Association postdoctoral fellowship 0225759T (to V. Sirotkin).

Submitted: 8 February 2005
Accepted: 13 July 2005

References

Anderson, B.L., I. Boldogh, M. Evangelista, C. Boone, L.A. Greene, and L.A. Pon. 1998. The Src homology domain 3 (SH3) of a yeast type I myosin, Myo5p, binds to verprolin and is required for targeting to sites of actin polarization. *J. Cell Biol.* 141:1357–1370.

Bahler, J., J.Q. Wu, M.S. Longtine, N.G. Shah, A. McKenzie III, A.B. Steever, A. Wach, P. Philippsen, and J.R. Pringle. 1998. Heterologous modules for efficient and versatile PCR-based gene targeting in *Schizosaccharomyces pombe*. *Yeast.* 14:943–951.

Blanchoin, L., K.J. Amann, H.N. Higgs, J.B. Marchand, D.A. Kaiser, and T.D. Pollard. 2000. Direct observation of dendritic actin filament networks nucleated by Arp2/3 complex and WASP/Scar proteins. *Nature.* 404: 1007–1011.

Carnahan, R.H., and K.L. Gould. 2003. The PCH family protein, Cdc15p, recruits two F-actin nucleation pathways to coordinate cytokinetic actin ring formation in *Schizosaccharomyces pombe*. *J. Cell Biol.* 162:851–862.

Chang, F., and M. Peter. 2002. Cell biology. Formins set the record straight. *Science.* 297:531–532.

Donnelly, S.F., M.J. Pocklington, D. Pallotta, and E. Orr. 1993. A proline-rich protein, verprolin, involved in cytoskeletal organization and cellular growth in the yeast *Saccharomyces cerevisiae*. *Mol. Microbiol.* 10:585–596.

Doyle, T., and D. Botstein. 1996. Movement of yeast cortical actin cytoskeleton visualized in vivo. *Proc. Natl. Acad. Sci. USA.* 93:3886–3891.

Engqvist-Goldstein, A.E., and D.G. Drubin. 2003. Actin assembly and endocytosis: from yeast to mammals. *Annu. Rev. Cell Dev. Biol.* 19:287–332.

Engqvist-Goldstein, A.E., C.X. Zhang, S. Carreno, C. Barroso, J.E. Heuser, and D.G. Drubin. 2004. RNAi-mediated Hip1R silencing results in stable association between the endocytic machinery and the actin assembly machinery. *Mol. Biol. Cell.* 15:1666–1679.

Evangelista, M., B.M. Klebl, A.H. Tong, B.A. Webb, T. Leeuw, E. Leberer, M. Whiteway, D.Y. Thomas, and C. Boone. 2000. A role for myosin-I in actin assembly through interactions with Vrp1p, Bee1p, and the Arp2/3 complex. *J. Cell Biol.* 148:353–362.

Geli, M.I., R. Lombardi, B. Schmelzl, and H. Riezman. 2000. An intact SH3 domain is required for myosin I-induced actin polymerization. *EMBO J.* 19:4281–4291.

Giardini, P.A., D.A. Fletcher, and J.A. Theriot. 2003. Compression forces generated by actin comet tails on lipid vesicles. *Proc. Natl. Acad. Sci. USA.* 100:6493–6498.

Goodson, H.V., B.L. Anderson, H.M. Warrick, L.A. Pon, and J.A. Spudich. 1996. Synthetic lethality screen identifies a novel yeast myosin I gene (MYO5): myosin I proteins are required for polarization of the actin cytoskeleton. *J. Cell Biol.* 133:1277–1291.

Hertzog, M., E.G. Yarmola, D. Didry, M.R. Bubb, and M.F. Carlier. 2002. Control of actin dynamics by proteins made of beta-thymosin repeats: the actobindin family. *J. Biol. Chem.* 277:14786–14792.

Higgs, H.N., and T.D. Pollard. 2001. Regulation of actin filament network formation through ARP2/3 complex: activation by a diverse array of proteins. *Annu. Rev. Biochem.* 70:649–676.

Higgs, H.N., L. Blanchoin, and T.D. Pollard. 1999. Influence of the C terminus of Wiskott-Aldrich syndrome protein (WASp) and the Arp2/3 complex on actin polymerization. *Biochemistry.* 38:15212–15222.

Ho, H.Y., R. Rohatgi, A.M. Lebensohn, M. Le, J. Li, S.P. Gygi, and M.W. Kirschner. 2004. Toca-1 mediates Cdc42-dependent actin nucleation by activating the N-WASP-WIP complex. *Cell.* 118:203–216.

Huckaba, T.M., A.C. Gay, L.F. Pantalena, H.C. Yang, and L.A. Pon. 2004. Live cell imaging of the assembly, disassembly, and actin cable-dependent movement of endosomes and actin patches in the budding yeast, *Saccharomyces cerevisiae*. *J. Cell Biol.* 167:519–530.

Hufner, K., H.N. Higgs, T.D. Pollard, C. Jacobi, M. Aepfelbacher, and S. Linder. 2001. The verprolin-like central (vc) region of Wiskott-Aldrich syndrome protein induces Arp2/3 complex-dependent actin nucleation. *J. Biol. Chem.* 276:35761–35767.

Iwaki, T., N. Tanaka, H. Takagi, Y. Giga-Hama, and K. Takegawa. 2004. Characterization of *end4*$^+$, a gene required for endocytosis in *Schizosaccharomyces pombe*. *Yeast.* 21:867–881.

Jonsdottir, G.A., and R. Li. 2004. Dynamics of yeast Myosin I: evidence for a possible role in scission of endocytic vesicles. *Curr. Biol.* 14:1604–1609.

Kaksonen, M., Y. Sun, and D.G. Drubin. 2003. A pathway for association of receptors, adaptors, and actin during endocytic internalization. *Cell.* 115:

475–487.

Lechler, T., A. Shevchenko, and R. Li. 2000. Direct involvement of yeast type I myosins in Cdc42-dependent actin polymerization. *J. Cell Biol.* 148: 363–373.

Lechler, T., G.A. Jonsdottir, S.K. Klee, D. Pellman, and R. Li. 2001. A two-tiered mechanism by which Cdc42 controls the localization and activation of an Arp2/3-activating motor complex in yeast. *J. Cell Biol.* 155: 261–270.

Lee, W.L., E.M. Ostap, H.G. Zot, and T.D. Pollard. 1999. Organization and ligand binding properties of the tail of Acanthamoeba myosin-IA. Identification of an actin-binding site in the basic (tail homology-1) domain. *J. Biol. Chem.* 274:35159–35171.

Lee, W.L., M. Bezanilla, and T.D. Pollard. 2000. Fission yeast myosin-I, Myo1p, stimulates actin assembly by Arp2/3 complex and shares functions with WASp. *J. Cell Biol.* 151:789–800.

Li, R. 1997. Bee1, a yeast protein with homology to Wiscott-Aldrich syndrome protein, is critical for the assembly of cortical actin cytoskeleton. *J. Cell Biol.* 136:649–658.

Machesky, L.M. 2000. The tails of two myosins. *J. Cell Biol.* 148:219–221.

Marchand, J.B., D.A. Kaiser, T.D. Pollard, and H.N. Higgs. 2001. Interaction of WASP/Scar proteins with actin and vertebrate Arp2/3 complex. *Nat. Cell Biol.* 3:76–82.

Martinez-Quiles, N., R. Rohatgi, I.M. Anton, M. Medina, S.P. Saville, H. Miki, H. Yamaguchi, T. Takenawa, J.H. Hartwig, R.S. Geha, and N. Ramesh. 2001. WIP regulates N-WASP-mediated actin polymerization and filopodium formation. *Nat. Cell Biol.* 3:484–491.

Merrifield, C.J. 2004. Seeing is believing: imaging actin dynamics at single sites of endocytosis. *Trends Cell Biol.* 14:352–358.

Merrifield, C.J., M.E. Feldman, L. Wan, and W. Almers. 2002. Imaging actin and dynamin recruitment during invagination of single clathrin-coated pits. *Nat. Cell Biol.* 4:691–698.

Mulholland, J., D. Preuss, A. Moon, A. Wong, D. Drubin, and D. Botstein. 1994. Ultrastructure of the yeast actin cytoskeleton and its association with the plasma membrane. *J. Cell Biol.* 125:381–391.

Munn, A.L. 2001. Molecular requirements for the internalisation step of endocytosis: insights from yeast. *Biochim. Biophys. Acta.* 1535:236–257.

Munn, A.L., B.J. Stevenson, M.I. Geli, and H. Riezman. 1995. end5, end6, and end7: mutations that cause actin delocalization and block the internalization step of endocytosis in *Saccharomyces cerevisiae*. *Mol. Biol. Cell.* 6:1721–1742.

Naqvi, S.N., R. Zahn, D.A. Mitchell, B.J. Stevenson, and A.L. Munn. 1998. The WASp homologue Las17p functions with the WIP homologue End5p/verprolin and is essential for endocytosis in yeast. *Curr. Biol.* 8:959–962.

Pelham, R.J., Jr., and F. Chang. 2001. Role of actin polymerization and actin cables in actin-patch movement in *Schizosaccharomyces pombe*. *Nat. Cell Biol.* 3:235–244.

Pollard, T.D., L. Blanchoin, and R.D. Mullins. 2000. Molecular mechanisms controlling actin filament dynamics in nonmuscle cells. *Annu. Rev. Biophys. Biomol. Struct.* 29:545–576.

Ramesh, N., I.M. Anton, J.H. Hartwig, and R.S. Geha. 1997. WIP, a protein associated with Wiskott-Aldrich Syndrome protein, induces actin polymerization and redistribution in lymphoid cells. *Proc. Natl. Acad. Sci. USA.* 94:14671–14676.

Rodal, A.A., L. Kozubowski, B.L. Goode, D.G. Drubin, and J.H. Hartwig. 2005. Actin and septin ultrastructures at the budding yeast cell cortex. *Mol. Biol. Cell.* 16:372–384.

Smith, M.G., S.R. Swamy, and L.A. Pon. 2001. The life cycle of actin patches in mating yeast. *J. Cell Sci.* 114:1505–1513.

Sokac, A.M., C. Co, J. Taunton, and W. Bement. 2003. Cdc42-dependent actin polymerization during compensatory endocytosis in Xenopus eggs. *Nat. Cell Biol.* 5:727–732.

Takagi, T., S.A. Ishijima, H. Ochi, and M. Osumi. 2003. Ultrastructure and behavior of actin cytoskeleton during cell wall formation in the fission yeast *Schizosaccharomyces pombe*. *J. Electron Microsc. (Tokyo).* 52: 161–174.

Upadhyaya, A., J.R. Chabot, A. Andreeva, A. Samadani, and A. van Oudenaarden. 2003. Probing polymerization forces by using actin-propelled lipid vesicles. *Proc. Natl. Acad. Sci. USA.* 100:4521–4526.

Vaduva, G., N.C. Martin, and A.K. Hopper. 1997. Actin-binding verprolin is a polarity development protein required for the morphogenesis and function of the yeast actin cytoskeleton. *J. Cell Biol.* 139:1821–1833.

Volkman, B.F., K.E. Prehoda, J.A. Scott, F.C. Peterson, and W.A. Lim. 2002. Structure of the N-WASP EVH1 domain-WIP complex: insight into the molecular basis of Wiskott-Aldrich Syndrome. *Cell.* 111:565–576.

Waddle, J.A., T.S. Karpova, R.H. Waterston, and J.A. Cooper. 1996. Movement of cortical actin patches in yeast. *J. Cell Biol.* 132:861–870.

Weaver, A.M., M.E. Young, W.L. Lee, and J.A. Cooper. 2003. Integration of signals to the Arp2/3 complex. *Curr. Opin. Cell Biol.* 15:23–30.

Wu, J.Q., J.R. Kuhn, D.R. Kovar, and T.D. Pollard. 2003. Spatial and temporal pathway for assembly and constriction of the contractile ring in fission yeast cytokinesis. *Dev. Cell.* 5:723–734.

Young, M.E., J.A. Cooper, and P.C. Bridgman. 2004. Yeast actin patches are networks of branched actin filaments. *J. Cell Biol.* 166:629–635.

Zacharias, D.A., J.D. Violin, A.C. Newton, and R.Y. Tsien. 2002. Partitioning of lipid-modified monomeric GFPs into membrane microdomains of live cells. *Science.* 296:913–916.

Zalevsky, J., L. Lempert, H. Kranitz, and R.D. Mullins. 2001. Different WASP family proteins stimulate different Arp2/3 complex-dependent actin-nucleating activities. *Curr. Biol.* 11:1903–1913.